On the rheological characterisation of liquefied sands through the dam-breaking test

Della Vecchia, Gabriele; Cremonesi, Massimiliano; Pisanò, Federico

DOI
10.1002/nag.2905

Publication date
2019

Document Version
Accepted author manuscript

Published in
International Journal for Numerical and Analytical Methods in Geomechanics

Received XXX; | Revised XXX; | Accepted XXX

DOI: xxx/xxxx

ARTICLE TYPE

On the rheological characterisation of liquefied sands through the dam breaking test

Gabriele Della Vecchia[1] | Massimiliano Cremonesi[1] | Federico Pisanò[2]

[1]Department of Civil and Environmental Engineering, Politecnico di Milano, Milano, Italy

[2]Faculty of Civil Engineering and Geosciences, Delft University of Technology, Delft, The Netherlands

Correspondence

*G. Della Vecchia, Piazza L. da Vinci 33, 20133 Milan (Italy). Email: gabriele.dellavecchia@polimi.it

Present Address

This is sample for present address text this is sample for present address text

Summary

This paper concerns the rheological characterisation of liquefied sands as non-Newtonian Bingham fluids. For this purpose, dam breaking laboratory tests are often executed and interpreted, offering a viable option to identify the properties of fluidised water-soil mixtures. However, limited attention has been devoted so far to clarify what variables and measurements would allow an unambiguous calibration of Bingham parameters, namely the viscosity η and the yield stress τ_y.

The numerical results of parametric studies based on the Particle Finite Element Method (PFEM) are critically inspected to gain deeper insight into the problem. First, it is confirmed that multiple $\eta - \tau_y$ pairs may reproduce the same experimental evidence when formed by only one measurement – usually, the post-dam-breaking displacement of the bottom toe (tip) of the liquefied mass. Then, two alternative procedures are proposed for a unambiguous identification of both η and τ_y: one is based on monitoring the evolving aspect ratio of the fluid mass during free, gravity-driven flow; the other relies on a slightly different dam breaking test, also including the impact of the liquefied soil against a rigid obstacle. In particular, the latter approach reduces the relevant duration of the test, mitigating the possible influence of re-consolidation effects on the calibration of rheological parameters.

KEYWORDS:

liquefied sands; rheology; Bingham fluid; dam breaking; CFD; PFEM

1 | INTRODUCTION

The term 'liquefaction' denotes the loss of shear strength and stiffness suffered by loose sandy soils in response to monotonic or cyclic stages of (nearly) undrained loading. Such a phenomenon is caused by the abrupt build-up of pore water pressure and the resulting decrease of effective stresses, leading the soil to behave as a viscous fluid until solid-like properties are eventually recovered through water drainage (re-consolidation)[1].

Catastrophic consequences of sand liquefaction are documented in the literature in relation to countless case studies, including foundation collapses under buildings and bridges[2,3,4], flow slides in earth slopes[5], failure of tailing dams[6], sinking/flotation of buried pipelines[7]. A number of constitutive models have been proposed in the literature to predict the onset of liquefaction under either monotonic or cyclic undrained loading, however with no use in terms of post-liquefaction evolution, i.e. when large deformation conditions weigh in. Some early works attempted the simulation of post-liquefaction flow in the framework of solid mechanics by adopting enhanced finite-strain constitutive relationships[8,9], up until the route of Computational Fluid Dynamics (CFD) was found better suited for interaction problems involving solid structures and fluidised geomaterials.

With very few exceptions of theoretical/analytical studies on permanent ground displacements [10] and submarine landslides [11], different numerical methods have been applied to a variety of relevant applications, including liquefaction-induced soil lateral spreading [12], flow failure of mine tailing dams [6], interaction of flowing masses with foundation piles [13] and debris avalanches [14]. For instance, Uzuoaka *et al.* [12] proposed a finite volume discretization on a staggered grid of Navier-Stokes governing equations based on a Semi Implicit Method for Pressure Linked Equation (SIMPLE) method. Hadush *et al.* [15] studied the lateral spreading of liquefied soils via a CIP (Cubic Interpolated Pseudoparticles) method, exploiting its capability to handle the interface flow among different objects in presence of both compressible and incompressible materials. To overcome the intrinsic difficulties associated with free-surface flow problems, Pastor *et al.* [16,14] and Huang *et al.* [17,18] resorted to SPH (Smoothed Particle Hydrodynamics) to model the flow of fluidised geomaterials. More recently, Schenkengel & Vrettos [19] embraced the framework of statistical mechanics and applied a Lattice Boltzmann method to simulate the liquefaction-induced flow observed in shaking table tests, slope failure, and around an embedded rigid wall. As further stressed later in this work, the so-called Particle Finite Element Method (PFEM) has also proven a very suitable CFD approach to free-surface flow problems [20,21], mostly due to the fully Lagrangian formulation/solution of the problem.

In the lack of well-established constitutive theories for geomaterials transiting from solid-like to fluid-like behaviour, the latter is most often modelled in CFD-type simulations via the rheological idealisation of non-Newtonian Bingham fluid [14]. This implies that no flow is possible while the magnitude of the deviatoric stress state is below a given threshold τ_y, beyond which fluid flow occurs according to a linear relationship between deviatoric stresses and strain rates governed by the viscosity η. Accordingly, the use of the Bingham model requires two material parameters to be identified, namely the viscosity and the yield stress. The relevance of reliable rheological characterisation is self-apparent and key to the solution of engineering problems, especially when no consensus has yet been achieved in the literature about the range of liquefied soil parameters [22,13], or about their correlation with other properties describing the pre-liquefaction solid state (e.g. relative density, fraction and mineralogy of fine particles, in situ effective stress state etc.). In the case of the residual strength of granular materials after liquefaction events, classical approaches rely on the back-calculated values from field case histories, as proposed by Stark & Mesri [23] and Olson & Stark [24]. The inherent uncertainties related to field conditions and measurements lead to prefer for rheological characterisation laboratory tests with controlled initial/boundary conditions. The rheological parameters of fluidised soils can generally be obtained through either dedicated laboratory devices (e.g. rheometric [25,26] and viscometric [22]), or the back-analysis of small-scale tests. As pointed out by Brezzi *et al.* [27], viscosimeters are usually adopted for fine-grained soils, while their application to coarser materials is generally quite limited. Furthermore, when the fluid to be characterised is a liquefied sand, the adopted device should also allow for liquefaction itself to be triggered prior to relevant measurements. This argument confirms the higher viability of rheological characterisation based on the back-analysis of small-scale tests, such as pulling bar tests [13], moving ball tests [28,13,29], slump tests [30,31,27], rotating drum [32] and dam breaking tests.

The dam breaking test represents one of the simplest and fastest options for rheological characterisation, based on monitoring/interpreting the free flow of a liquefied sand mass. The test is executed in two simple stages: (i) first, a mass of liquefied soil is kept at rest against the fixed wall of a rigid container by a removable vertical baffle; (ii) then, the barrier is swiftly removed so as to allow the gravity-driven flow of the material – along either a horizontal or inclined floor surface. Typical experimental measurements track the time evolution of the tip displacement and/or of the free surface. At notable variance with real field cases, dam breaking tests performed in a laboratory environment enable full control of relevant initial and boundary conditions, which makes these tests particularly amenable to numerical simulation and back-analysis. Importantly, dam breaking experiments are purposely performed in a bidimensional setting. A single digital camera is thus sufficient to record the evolution of the flowing mass in the vertical plan, and simpler 2D models are fully suitable for its numerical simulation.

This paper targets a substantial improvement of dam breaking test interpretation as a key step towards the accurate characterisation of liquefied sands as Bingham fluids. For this purpose, parametric CFD-PFEM studies have been performed and their results critically inspected. When carefully interpreted, CFD results allow to clearly link the main features of dam breaking flow to the Bingham parameters of the liquefied sand, as well as to remove poorly documented ambiguities in existing interpretation procedures. As a main outcome, this work establishes two alternative approaches to obtain from dam breaking test measurements a single pair of viscosity and yield stress values for sands considered in their fully liquefied state.

2 | BINGHAM MODELLING OF LIQUEFIED SANDS

Despite some valuable recent efforts[33,34], a unified constitutive theory capable of describing both the solid-like and fluid-like behaviour of granular materials has not yet been achieved. This knowledge gap preserves the high relevance of the CFD framework to the analysis of fluidised geomaterials, in combination with rheological models that describe the behaviour of water-soil fluid mixtures by relating stresses and strain-rates – e.g. τ and $\dot{\gamma}$ in the case of uniaxial shear flow. For mixtures with high sediment concentration a linear rheological law can be assumed beyond a material-specific 'yield stress' threshold[22]. The presence of a yield stress below which no fluid flow occurs implies the overall non-linearity of the rheological model, commonly referred to as non-Newtonian. Several non-Newtonian formulations are available in the literature, among which the Bingham model has gained over the years the widest popularity for applications involving liquefied sands[17,35]. The popularity of the Bingham model does not only arise from its simplicity, but also from the existing bulk of experimental data in its support – as shown by O'Brien & Julien[22] for fine-grained materials, and Nishimura et al.[36] and by Gallage et al.[37] for liquefied sands.

TABLE 1 Previous applications of fluid modelling to the flow of water-soil mixtures.

Authors	Rheological model	Application
Jeyapalan et al.[6]	Bingham	Dam breaking
Uzuoka et al.[12]	Bingham	Dam breaking
Hadush et al.[38]	Pseudo-plastic, Bingham	Dam breaking
Hadush et al.[15]	Bingham	Dam breaking
Moriguchi et al.[39]	Bingham (frictional)	Dam breaking
de Alba & Ballestero[29]	Bingham	Moving bar
Pastor et al.[40]	Viscoplastic	Landslide
Moriguchi et al.[35]	Bingham (frictional)	Dam breaking
Huang et al.[17]	Bingham (frictional)	Dam breaking
Pastor et al.[14]	Bingham, Viscoplastic	Landslide

Under pure shear flow conditions, Bingham's model is represented by the simple uniaxial relationship between shear stress and shear strain rate:

$$\begin{cases} \tau = \tau_y + \eta\dot{\gamma} \equiv \eta'\dot{\gamma} & \text{if} \quad \tau > \tau_y \\ \dot{\gamma} = 0 & \text{otherwise} \end{cases} \tag{1}$$

where the material parameters η and τ_y represent the phenomenological viscosity and yield stress of the liquefied soil. Equation (1) also shows how the same relationship can be recast into a Newtonian linear form through the definition of an equivalent, strain-rate–dependent viscosity η':

$$\eta' = \begin{cases} \eta + \dfrac{\tau_y}{\dot{\gamma}} & \text{for} \quad \dot{\gamma} > 0 \\ \to \infty & \text{for} \quad \dot{\gamma} = 0 \end{cases} \tag{2}$$

which is in line with the wide experimental evidence concerning the non-Newtonian nature of liquefied soils[15]. The multi-axial generalisation of Equations (1)-(2) for 2D/3D problems is straightforward and reads as[41]:

$$\begin{cases} s_{ij} = \tau_y \dfrac{\dot{\epsilon}_{ij}}{\left\|\dot{\epsilon}_{ij}\right\|} + 2\eta\dot{\epsilon}_{ij} \equiv 2\eta'\dot{\epsilon}_{ij} & \text{if} \quad \left\|\tau_{ij}\right\| > \tau_y \\ \dot{\epsilon}_{ij} = 0 & \text{otherwise} \end{cases} \quad \Rightarrow \quad \eta' = \begin{cases} \eta + \dfrac{\tau_y}{2\left\|\dot{\epsilon}_{ij}\right\|} & \text{for} \quad \left\|\dot{\epsilon}_{ij}\right\| > 0 \\ \to \infty & \text{for} \quad \left\|\dot{\epsilon}_{ij}\right\| = 0 \end{cases} \tag{3}$$

where s_{ij} and $\dot{\varepsilon}_{ij}$ are the tensors of deviatoric stress and strain rate, respectively, whereas relevant tensor norms are defined as $\left\|\tau_{ij}\right\| = \sqrt{(1/2)\, s_{ij} s_{ij}}$ and $\left\|\varepsilon_{ij}\right\| = \sqrt{(1/2)\, \dot{\varepsilon}_{ij} \dot{\varepsilon}_{ij}}$. The Bingham model sets a relationship between the deviatoric components of stress and strain rate tensors, while the hydrostatic mean pressure emerges from assumptions concerning the compressibility of the fluid. In the following, incompressible fluid flow will be exclusively considered[1], which is also consistent with assumption of fully undrained conditions during post-liquefaction motion.

Refinements of the basic Bingham model have been also proposed to include a pressure-dependent yield stress (e.g. $\tau_y = \tau_{y0} + p \tan\phi$), thus introducing an additional parameter to calibrate. In light of its simplicity, the Bingham model has been widely applied to geotechnical problems; this is clearly witnessed by the literature review summary in Table 1, where relevant studies on the flow of soil-water mixtures are mentioned along with the rheological model adopted. The Bingham model is also adopted in this study with focus on the objective identification of its free parameters (η and τ_y – Equation 1) through dam breaking experiments.

3 | NUMERICAL SIMULATION OF DAM BREAKING TESTS

All CFD simulations have been carried out based on the Particle Finite Element Method (PFEM), in the version developed and implemented by Cremonesi *et al.*[42,41]. The PFEM has been widely used in engineering applications, such as free-surface fluid dynamics[20,21], fluid-structure interaction[43,44,45], bed erosion[46], manufacturing processes[47], landslides[48] and granular flows[49]. In particular, the method relies on a fully Lagrangian description of free-surface fluid flow, and has been proven especially suitable for the simulation of fluid-structure interaction. The fluid mass is assumed to flow as a viscous incompressible fluid during the time interval $(0, T)$, with the conservation of linear momentum and mass associated with the following Navier-Stokes equations over the moving volume Ω_t:

$$\begin{aligned} \rho \frac{Du_i}{Dt} &= \sigma_{ij,j} + \rho b_i \quad \text{in } \Omega_t \times (0,T) \\ u_{i,i} &= 0 \quad \text{in } \Omega_t \times (0,T) \end{aligned} \tag{4}$$

where Du_i/Dt represents the material time derivative operator applied to each component of local velocity u_i, σ_{ij} the Cauchy stress tensor, ρ the mass density and b_i the external body force vector. The Cauchy stress tensor can be conveniently decomposed into deviatoric (s_{ij}) and isotropic components (p, mean pressure):

$$\sigma_{ij} = s_{ij} - p\delta_{ij} \tag{5}$$

where δ_{ij} is the second-order identity tensor and the mean pressure p (positive when compressive).

The above governing equations in their fully Lagrangian form are then discretised in space according to the classical Galerkin Finite Element approach, based on a linear equal-order nodal interpolation of both fluid pressure and velocity. The following semi-discrete system of ordinary differential equations results:

$$\mathbf{M}\dot{\mathbf{U}} + \mathbf{K}\mathbf{U} + \mathbf{D}^T\mathbf{P} = \mathbf{B} \tag{6}$$

$$\mathbf{D}\mathbf{U} = \mathbf{0} \tag{7}$$

where the vectors $\mathbf{U}$ and $\mathbf{P}$ contain the nodal values of velocity components and pressure respectively, whereas $\mathbf{M}$ is the mass matrix, $\mathbf{K}$ the Bingham rheological/stiffness matrix, $\mathbf{D}$ the discrete divergence operator, $\mathbf{B}$ the vector of external body forces and boundary tractions – full description of the above matrices/vectors is available in Cremonesi[50].

Starting from pre-set initial conditions, time marching from t_n to t_{n+1} is performed by applying the implicit backward Euler integration scheme to the above semi-discrete, non-linear system of equations:

$$\left(\frac{\mathbf{M}}{\Delta t} + \mathbf{K}\right)\mathbf{U}^{n+1} + \mathbf{D}^T\mathbf{P}^{n+1} = \mathbf{B}^{n+1} + \frac{\mathbf{M}}{\Delta t}\mathbf{U}^n \tag{8}$$

$$\mathbf{D}\mathbf{U}^{n+1} = \mathbf{0} \tag{9}$$

Following Idelsohn *et al.*[51], each simulation step is solved iteratively via a Picard algorithm, here preferred over the standard Newton-Raphson scheme. Accordingly, a simple fixed point method is applied at each k^{th} iteration to evaluate the relevant matrices emerging from Equations (8)–(9) at a configuration estimated at the $(k-1)^{th}$ iteration.

[1] During incompressible flow, the total strain rate tensor $\dot{\varepsilon}_{ij}$ coincides with its deviatoric component.

The proposed numerical approach is based on a mixed formulation in which velocity and pressure play as independent variables. When the governing equations are discretised in space, the approximation spaces for pressure and velocity cannot be defined independently, but should fulfil the so-called *inf-sup* (or LBB) condition. This implies a restriction on the compatibility between the approximations of the two unknown variables. It is also possible to overcome the inf-sup condition (and the extra computational burden it normally causes) by means of a stabilised reformulation of the original problem. Indeed, this path is followed in the adopted Particle Finite Element Method (PFEM), in which linear/equal-order nodal interpolation of both velocity and pressure is set to guarantee very fast and efficient remeshing during large deformation. This choice would not per se fulfill the inf-sup condition, so that the so-called *pressure-stabilising/Petrov-Galerkin* (PSPG) stabilization is introduced[52], as explained in Cremonesi et al[42].

In the spirit of the PFEM, re-meshing is frequently performed to mitigate the mesh distortion sponstaneously arising from the Lagrangian formulation of large deformation problems. A suitable index of element distortion is used to monitor the need for mesh regeneration: whenever a new mesh has to be created (see Fig. 1a), a Delaunay tessellation technique is used to redefine the element connectivities starting from the current nodal positions (see Figure 1b); moreover, an "alpha-shape" technique is introduced to identify free-surfaces (see Figure 1c), according to the approach detailed in Cremonesi et al[41,42].

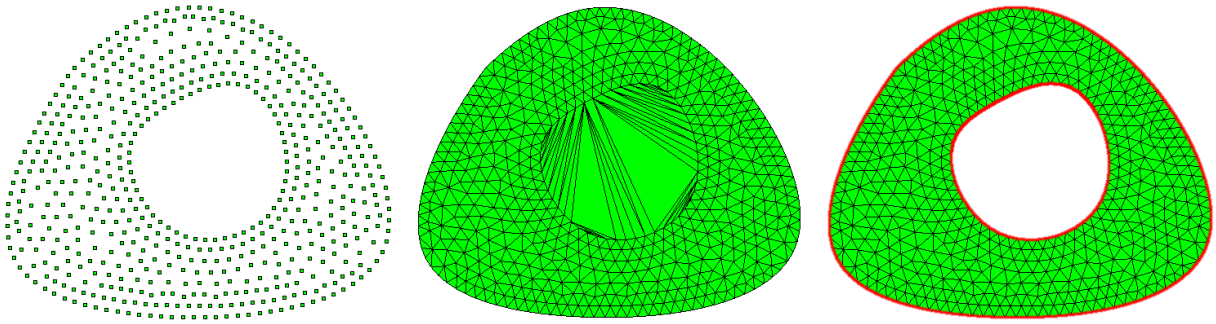

(a) PFEM: initial point distribution **(b)** PFEM: Delaunay tessellation **(c)** PFEM: Delaunay tessellation and alpha-shape technique

FIGURE 1 PFEM redefinition of mesh connectivities: Delaunay tessellation and alpha shape technique: (a) PFEM: initial point distribution; (b) PFEM: Delaunay tessellation; (c) PFEM: Delaunay tessellation and alpha-shape technique.

From a geotechnical standpoint, the assumption of incompressible one-phase flow can be regarded as a "total stress analysis" of dam breaking: no distinction is made between solid and fluid phases, while undrained/isochoric conditions are maintained during the motion of the liquefied soil mass – i.e. transient re-consolidation is neglected.

All PFEM simulations of dam breaking in this work refer to the set-up shown in Figure 2. The fluid mass is initially at rest in a rectangular configuration (initial width L_0 and height H_0), then let free to move under the gravity acceleration field. 2D plain strain numerical simulations have been performed by discretising the liquefied soil domain with 3-node triangular elements. Velocity no-slip boundary conditions have been set along all container walls, with constant pressure imposed at the free surface of the flowing mass – no surface tension considered. Parametric analyses concerning space-time discresation have been initially performed to ensure the accuracy of the numerical solution while trading off on the associated computational costs. Figure 3 exemplifies the evolution of an initial mesh set-up as induced by free-surface flow and related re-meshing – the effectiveness of the "alpha-shape" technique in maintaining suitable element shapes upon re-meshing should particularly be noted.

4 | MODEL PREDICTIONS AND CALIBRATION DILEMMA

The above PFEM model has been first used to reproduce the experimental results provided by Huang et al.[17]. These authors performed a dam breaking test on saturated sand, brought to liquefaction through the 1 Hz vibration of a shaking table. The sand sample used for the experiment (mean particle size: 0.24 mm) was prepared in the dam breaking box at a dry density of 1510 kg/m^3, with the following relevant sizes as termed in Figure 2: $L_{box} = 98$ cm, $H_{box} = 35$ cm, $L_0 = 32$ cm and $H_0 = 26.7$ cm. After sand liquefaction, the vertical baffle was removed and the material flow recorded by means of a high-speed camera. The experimental results in Figure 4 illustrate the horizontal position of the liquefied mass tip against time, over a total duration of 6

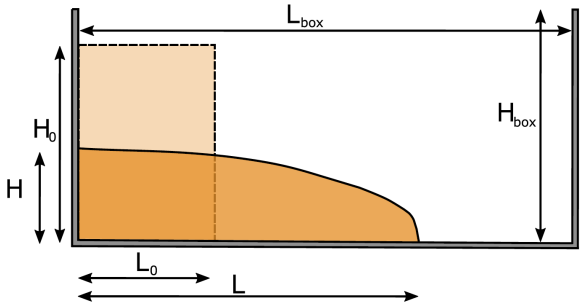

FIGURE 2 Dam breaking test: set-up and geometry

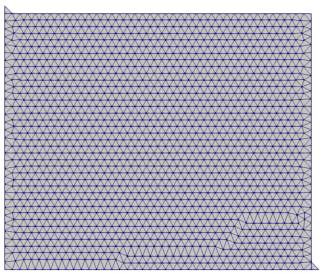

(a) initial mesh configuration

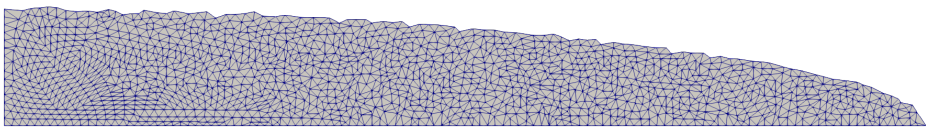

(b) final mesh configuration

FIGURE 3 Mesh evolution due to fluid flow and related re-meshing: (a) initial and (b) final (steady state) mesh configuration.

s. PFEM simulations of the test have been executed with a mesh including 3000 nodes and a time-step size $\Delta t = 0.001$ s. Related velocity contour plots are shown in Figure 5 at different time steps. The maximum shear strain resulting from all simulations is in the order of 0.1 $1/s$, which is well below the strain rate lower bound identified experimentally by O'Brien & Julien[22] for the applicability of Bingham modelling.

With no rheological characterisation available for the liquefied material, its density (ρ) viscosity (η) and yield stress (τ_y) have been calibrated to best-fit the experimental data. However, even after pre-setting the mass density to $\rho = 1600$ kg/m^3, it has not been possible to identify a unique $\eta - \tau_y$ pair: Figure 4 confirms that simulations of comparable quality can be achieved with two quite different sets of Bingham parameters. Similar predictions can be also obtained with different sets of rheological parameters, namely larger viscosities associated with lower yield stresses.

On the same token, Figure 6 shows the outcome of a parametric study on the simulation of Huang *et al.*'s[17] test with either (i) varying viscosity ($\eta \in$ [100;800] Pa·s) and constant $\tau_y = 20$ Pa, or (ii) varying yield stress ($\tau_y \in$ [20;400] Pa) and constant $\eta = 400$ Pa·s). It is apparent that variations of either η or τ_y produce similar qualitative effects on the position of the moving

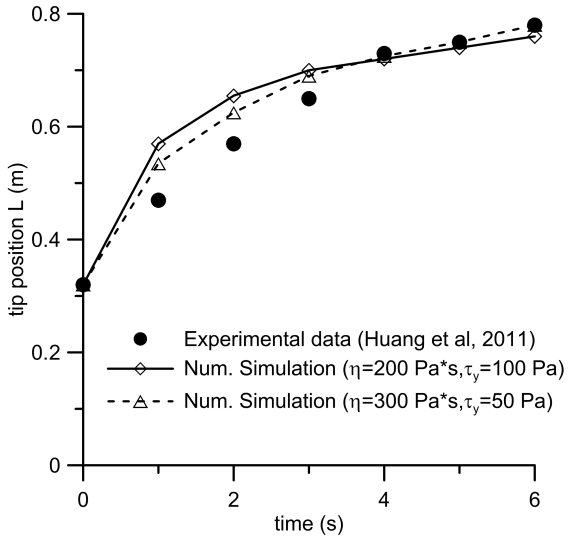

FIGURE 4 Position of the liquefied mass tip vs time: PFEM simulation vs. experimental data from Huang *et al.*[17]

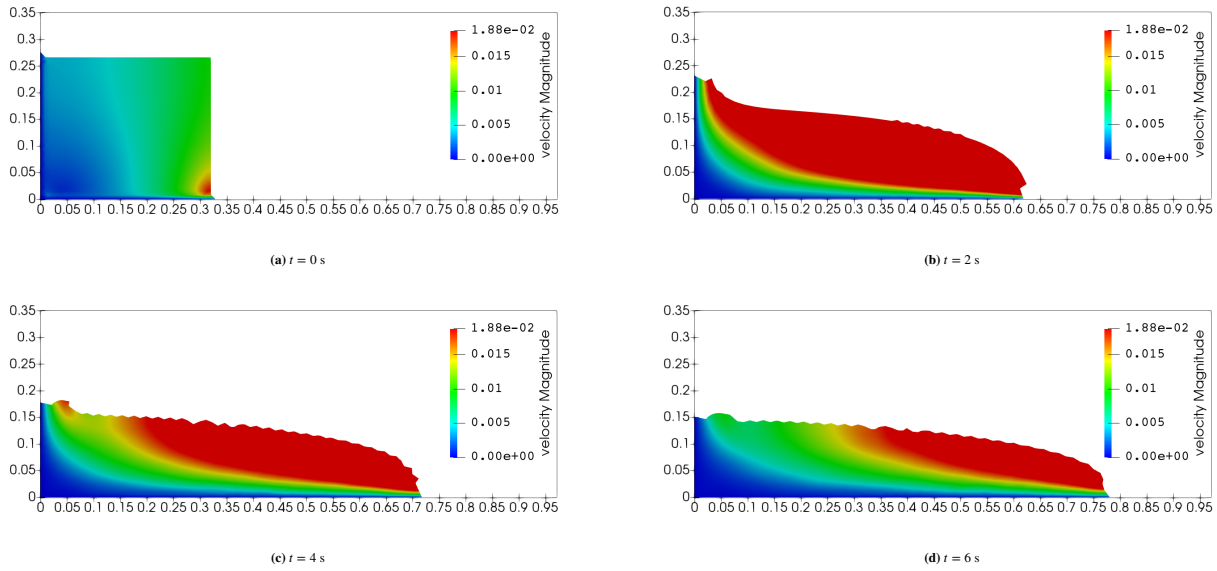

FIGURE 5 Velocity contour plots – values in m/s. Set of material parameters: $\rho = 1600$ kg/m^3, $\eta = 300$ Pa·s, $\tau_y = 50$ Pa: (a) $t = 0$ s; (b) $t = 2$ s; (c) $t = 4$ s; (d) $t = 6$ s.

tip, in a way that makes practically impossible to identify both parameters by only looking at one specific measurment. Similar conclusions have also been drawn by Jeyapalan *et al.*[6] and Moriguchi *et al.*[39], still regarding the simulation of dam breaking tests. Although conceptually obvious, such a "calibration dilemma" has not yet found a satisfactory solution – the remainder of this paper is fully devoted to filling this relevant gap.

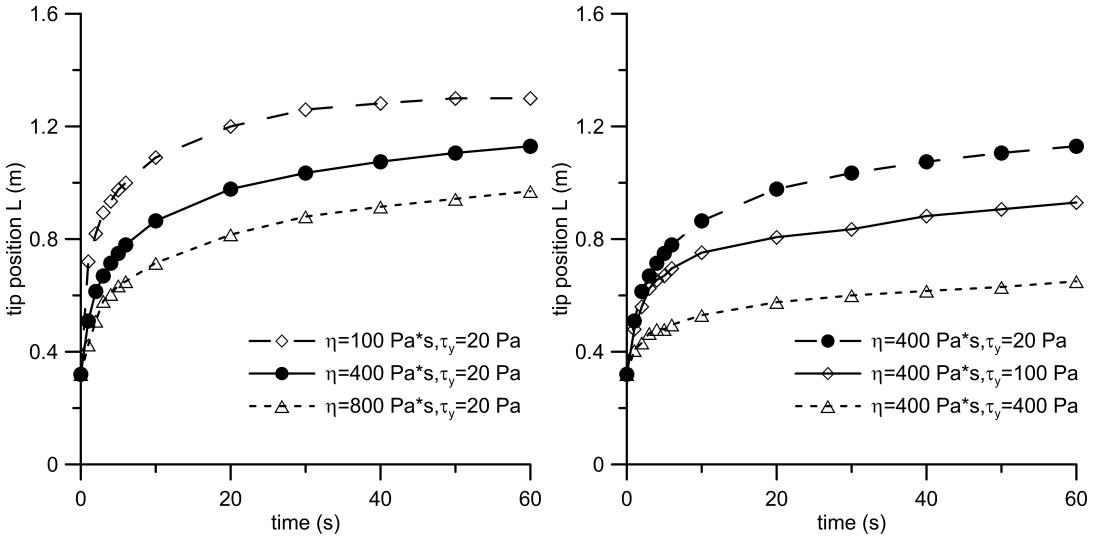

(a) varying viscosity, constant yield stress

(b) varying yield stress, constant viscosity

FIGURE 6 Sensitivity of dam breaking PFEM results to viscosity and yield stress – time evolution of tip position: (a) varying viscosity, constant yield stress; (b) varying yield stress, constant viscosity.

5 | UNAMBIGUOUS IDENTIFICATION OF BINGHAM PARAMETERS

5.1 | From the analysis of free, gravity-driven flow

More robust calibration of Bingham parameters can be achieved by monitoring at the same time the position of the mass tip and the maximum height at the back-wall, i.e. L and H in Figure 2, with the latter decreasing in time as the liquefied material flows. In particular, useful indications may be obtained from the time evolution of the H/L aspect ratio. After simple post-processing of the same results as in Figure 6, Figure 7 shows how the effects of varying η and τ_y are more readily apparent when visualized in terms of H/L ratio: a varying τ_y at constant η directly impacts the final steady state value of the aspect ratio, whereas a varying η at constant τ_y results in different evolution rates towards approximately the same asymptotic H/L value (Figure 7b). Unlike the time evolution of the tip displacement, the asymptotic H/L ratio appears to be barely affected by the material viscosity – see Figure 7b. In order to highlight this finding, numerical simulations have been run up to a physical time of 100 seconds – a significant interval compared to the typical duration of dam breaking tests. It should also be recalled that Bingham's constitutive equations (3) are perfectly compatible with $\lim_{t\to\infty} H > 0$: the ability to mobilise shear at rest allows for a non-horizontal free surface as static equilibrium is approached[53].

The negligible influence of viscosity on the asymptotic H/L value is confirmed in Figure 8a with respect to a different yield stress, namely $\tau_y = 100$ Pa. The alternative semi-logarithmic representation in Figure 8b remarks the role of viscosity to be most relevant just in the early stage of dam breaking flow.

From a geotechnical standpoint, the time needed for the H/L ratio to reach its steady state value would deserve further discussion. The case of liquefied sands seems quite delicate in this respect, as a meaningful characterisation of fluid-like behaviour should concern a time-window preceding re-consolidation. Experimental data from the literature illustrate that the time needed for the inception of pore pressure dissipation is hardly larger than 1–2 minutes under typical testing conditions[29,54,55] – although with prominent roles played by domain size and boundary conditions. The theoretical analyses by Balmforth *et al.*[56] and Matson & Hogg[57] show that both H and L tend to reach η-insensitive asymptotic values at steady state, although with a timing likely to let some re-consolidation to occur. Conversely, it can be proven[58] that the H/L ratio evolves much faster towards its steady state, which makes such a variable better suited for the rheological characterisation of fully liquefied sands. Nevertheless, it appears extremely challenging at the present state of the art to provide solid guidance on the timing of re-consolidation in flowing soil masses, a process happening in dam breaking tests as in real flowslides. This suggests that any measures reducing the meaningful duration of dam breaking tests can only be beneficial.

The link between the yield stress τ_y and the asymptotic H/L ratio has been parametrically explored for τ_y ranging from 50 Pa to 400 Pa at constant viscosity $\eta = 400$ Pa·s: the black markers in Figure 9 represent single PFEM simulations, while the

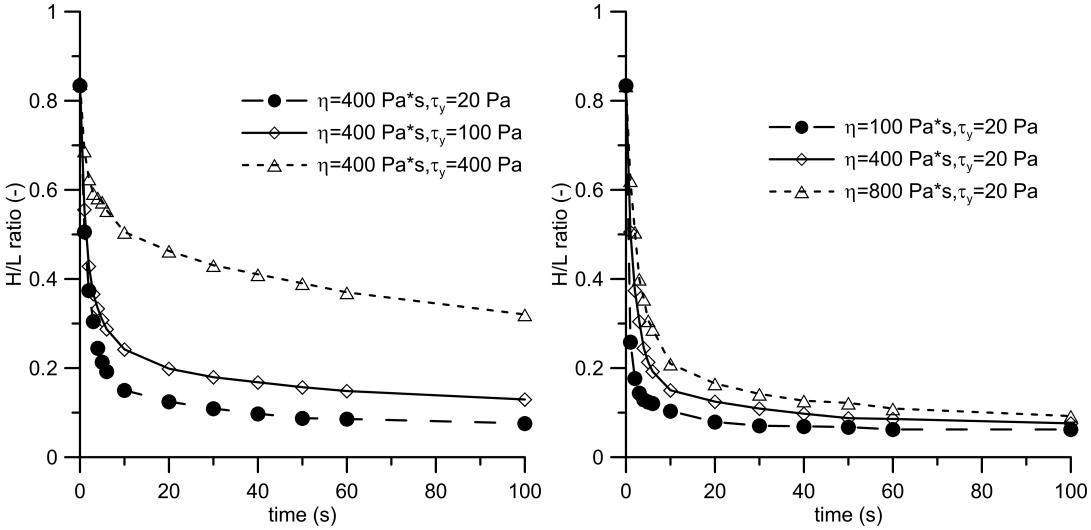

(a) varying yield stress, constant viscosity **(b)** varying viscosity, constant yield stress

FIGURE 7 Sensitivity of dam breaking PFEM results to viscosity and yield stress: time evolution of the H/L ratio: (a) varying yield stress, constant viscosity; (b) varying viscosity, constant yield stress.

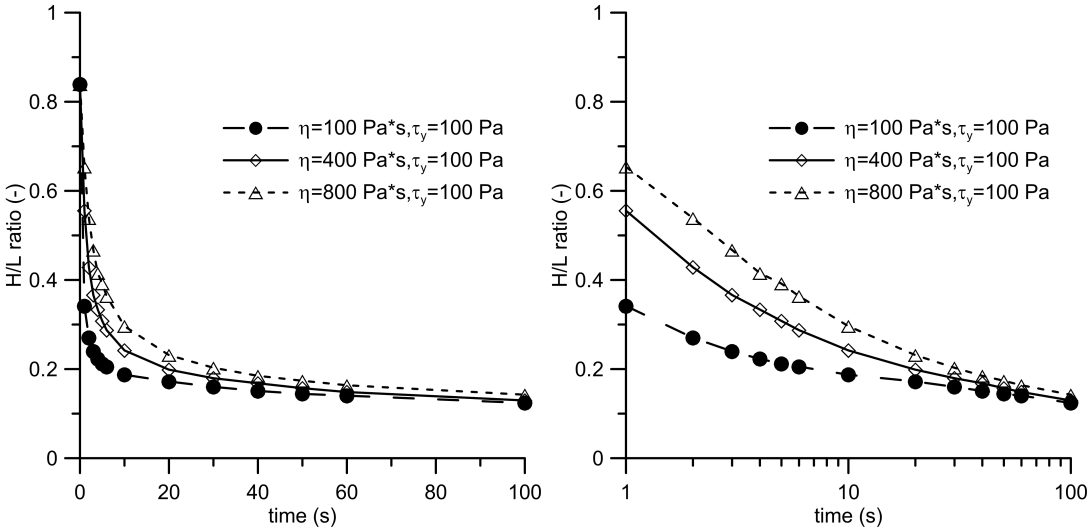

(a) varying viscosity, constant yield stress(τ_y = 100 Pa) **(b)** varying viscosity, constant yield stress(τ_y = 100 Pa), time in logarithmic scale

FIGURE 8 Sensitivity of dam breaking PFEM results to viscosity: time evolution of the H/L ratio for $\tau_y = 100$ Pa: (a) varying viscosity, constant yield stress($\tau_y = 100$ Pa); (b) varying viscosity, constant yield stress($\tau_y = 100$ Pa), time in logarithmic scale.

dashed interpolation line is associated with a very successful linear regression – coefficient of determination $R^2 = 0.9997$. Given the negligible influence of η, Figure 9 sets the ground for a unambiguous calibration of τ_y based on the asymptotic H/L ratio associated with the initial configuration H_0–L_0.

A more effective normalisation of numerical results can be achieved through a more general dimensionless variable B, also including the effect of the material density ρ and initial geometrical configuration $H_0 - L_0$:

$$B = \frac{\tau_y}{\rho g H_0} \frac{L_0}{H_0}, \tag{10}$$

in which g denotes the gravity acceleration. To stress the benefits of normalising dam breaking results through B, additional PFEM simulations have been performed for $\tau_y \in [50; 400]$ Pa, $\eta = 400$ Pa·s and four different fluid densities, namely$\rho =$

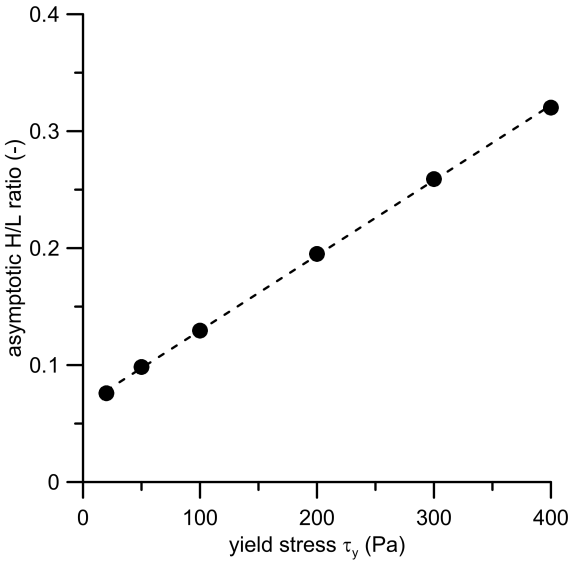

FIGURE 9 Relationship between asymptotic H/L ratio and yield stress τ_y for $\eta = 400$ Pa·s

1500, 1600, 1700, 1800 kg/m^3. As illustrated in Figure 10a, each density value a linear relation between τ_y and asymptotic H/L has been found, each one characterised by a specific slope in the relevant plane. Remarkably, when the same numerical results are re-plotted as a function of the aforementioned variable B, one single trend line can be identified – the linear regression line drawn in Figure 10b features a coefficient of determination $R^2 = 0.9988$.

The above arguments lead to conclude that monitoring the aspect ratio of the moving fluid mass can fruitfully support the unambiguous identification of η and τ_y with no extra-costs compared to standard interpretation procedures – indeed, the same images taken during the experiment provide both L and H at once. A robust calibration procedure distinguishing the roles played by τ_y and η can be established in two simple steps:

1. identify the yield stress from the experimental steady-state value of the (H/L) ratio – owing to the linearity of the trend in Figure 10b, only two numerical simulations are needed to obtain the relevant calibration curve associated with a specific initial geometry;

2. given τ_y, the experimental time evolution of the tip position can be best-fitted by setting an appropriate value of viscosity η sought over a realistic range – see Figure 6a.

Once more, it is worth remarking the simplicity of the proposed procedure, corroborated by the results of previous theoretical studies and state-of-the-art CFD-PFEM simulations.

5.2 | From the analysis of the impact on a rigid obstacle

As previously noted, Bingham parameters should be calibrated against experimental data representative of sand flow in its fully liquefied regime (before re-consolidation). However, real situations are envisaged in which the attainment of an asymptotic H/L ratio may be incompatible with such requirement. This drawback could be overcome by narrowing the time window over which relevant measurements are gathered, for instance by studying the impact of the liquefied mass against a rigid obstacle after dam breaking[59].

This procedure seems particularly suitable in presence of fast re-consolidation, as impact tests can provide valuable information in only a few seconds, a time shorter than needed to attain the asymptotic H/L ratio during free flow. Further, it is shown in the following that η and τ_y can be resolved even more clearly through the analysis of impact events.

With reference to the same set-up described by Huang *et al.*[17], the time evolution of the fluid pressure at a point P in contact with a vertical rigid obstacle is monitored, at distance d_P from the baffle and elevation h_P – see in Figure 11a. Hereafter, the discussion is carried out regarding the results of PFEM simulations performed with $d_P = 0.28$ m and $h_P = 0.016$ m.

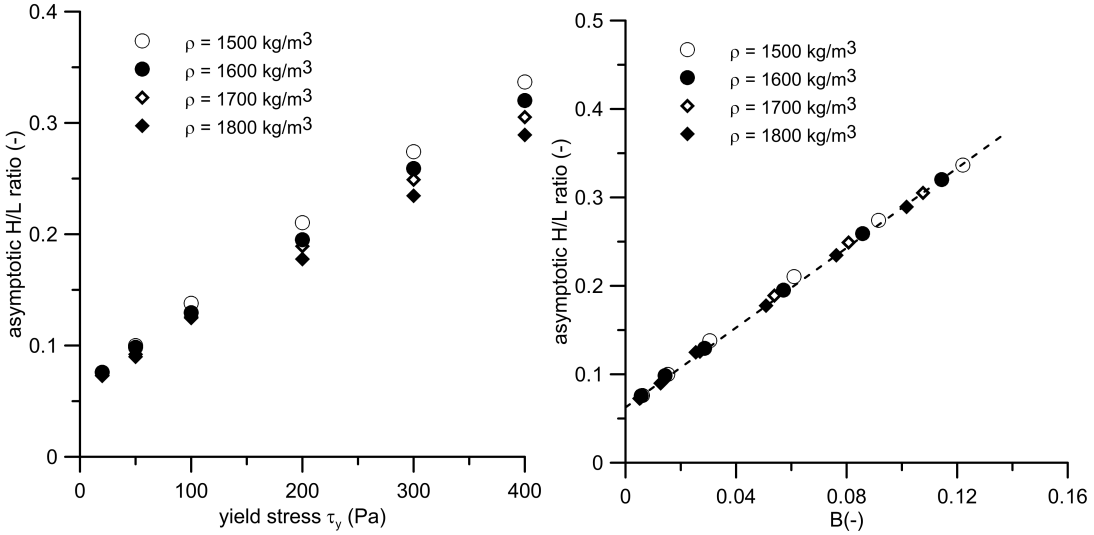

(a) Asymptotic H/L ratio vs. yield stress

(b) Asymptotic H/L ratio vs. B

FIGURE 10 Dependence of the asymptotic H/L ratio on the yield stress τ_y at varying material density: (a) Asymptotic H/L ratio vs. yield stress; (b) Asymptotic H/L ratio vs. B

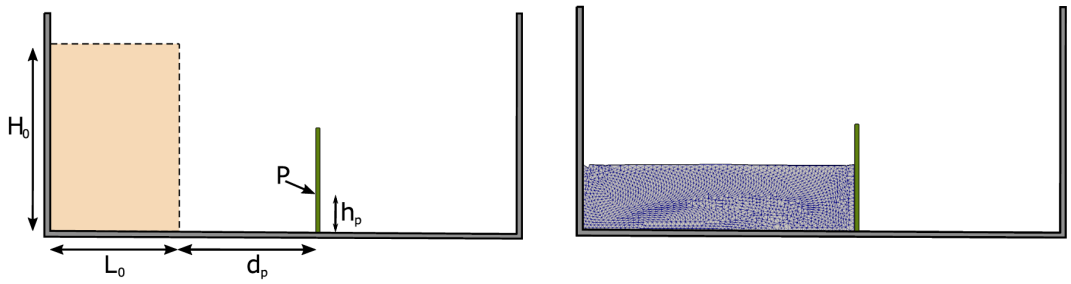

(a) Set-up and geometry

(b) Deformed mesh after soil mass stabilization

FIGURE 11 Dam breaking test with obstacle

Figure 12 depicts the time evolution of the fluid pressure at point P (p_P) for different viscosities and two distinct yield stresses ($\tau_y = 20$ Pa in Figure 12a and $\tau_y = 100$ Pa in Figure 12b). Since slower fluid motion results from increasing values of viscosity, a positive correlation is to be expected, for a given fluid density, between the time taken to impact the obstacle (impact time Δt_P) and the viscosity. Figure 13 confirms such expectation and shows that the $\Delta t_P - \eta$ correlation is very well represented by a linear regression line – in this case with a coefficient of determination $R^2 > 0.998$ for both yield stresses considered. Conversely, Figure 12 supports the inference that η has no effect on the final value of p_P, and opens to a two-stage calibration procedure in which η and τ_y are decoupled and separately identified. Importantly, the whole process including dam breaking, obstacle impact and final arrest takes place in only a few seconds, which leads closer to the assumption of fully liquefied regime.

Unlike the viscosity, the yield stress affects pronouncedly the final value of p_P. In this respect, Figure 14 illustrates the time evolutions of p_P associated with different yield stresses at two distinct viscosities ($\eta = 200$ Pa·s and $\eta = 400$ Pa·s): the strong effect of τ_y on the final value of p_P appears to be decoupled from the specific viscosity, as further visualised in Figure 15. Also in this case a linear regression trend works satisfactorily, with confirmed no effect of the viscosity. From a physical standpoint, τ_y affects the final configuration of the liquefied mass in terms of limit inclination of the free surface and, as a consequence, maximum elevation above the container floor. For instance, it could be easily verified in Figure 15 that the asymptotic p_P for $\tau_y \to 0$ (Newtonian fluid, no shear strength at rest) tends to the hydrostatic pressure under a flat free surface – i.e. $p_P\,(t \to \infty) = \rho g(h_\infty - h_P)$, where simple mass conservation arguments imply that $L_0 \cdot H_0 = \left(L_0 + d_P\right) \cdot H_\infty$ (Figure 11a). It should be mentioned that, for the ranges of viscosity, yield stress and density typical for fluidized soils (e.g. $\tau_y > 20$ Pa, $\eta > 20$

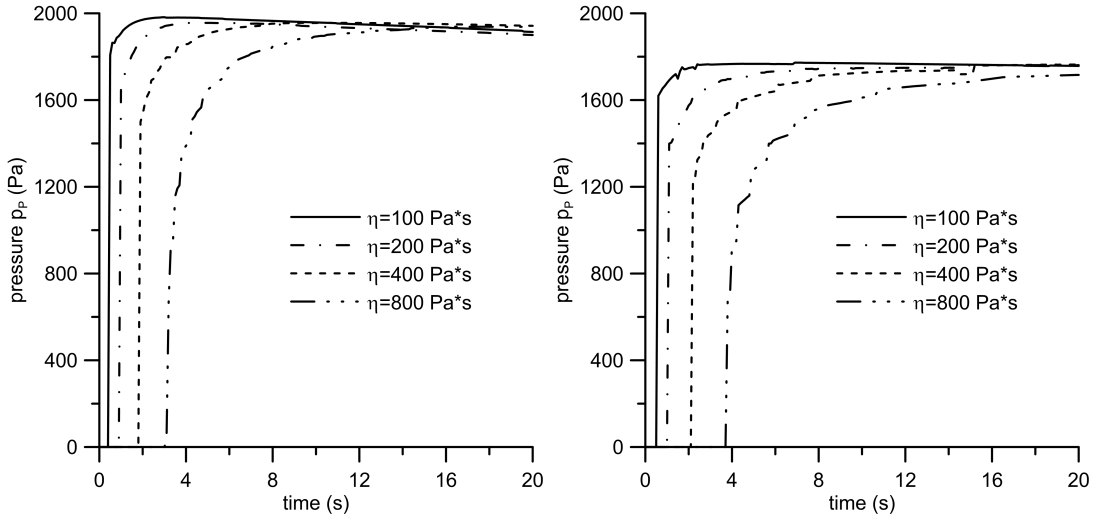

(a) Yield stress $\tau_y = 20$ Pa **(b)** Yield stress $\tau_y = 100$ Pa

FIGURE 12 Time evolution of the pressure p_P at varying viscosity: (a) Yield stress $\tau_y = 20$ Pa; (b) Yield stress $\tau_y = 100$ Pa

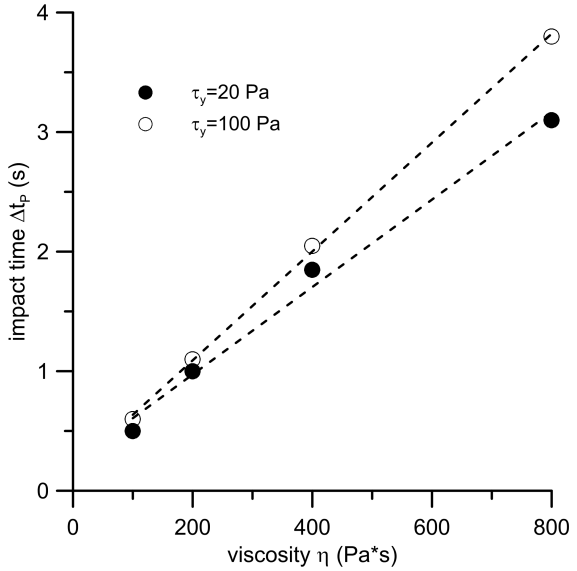

FIGURE 13 Dependence of the impact time Δt_P on the viscosity for two different yield stresses

Pa·s, ρ between 1500 and 1800 kg/m^3), the time evolution of the pressure on the obstacle can be either monotonically increasing or showing some decrease after a slight peak, as is evident in Figure 14a. This effect arises from small differences in the global dynamics of the flowing mass at different fluid viscosity and/or yield stress, which may imply different velocities at the time of the impact. The mentioned peak in the pressure time evolution, however, does not have any influence on the stationary value eventually attained (see Figures 12a and 13), nor, as a consequence, on the proposed calibration procedure.

Also in this alternative test set-up it is possible to normalize relevant correlations with respect to the density of the liquefied sand and its initial geometry. For this purpose, two dimensionless groups – the variable B and the normalised pressure $p/(\rho g H_0)$ – can be fruitfully exploited. Figure 16 shows that, for different fluid densities ρ taken in the range from 1500 to 1700 kg/m^3, all the simulation results regarding final p_P values lie on a single linear regression line – featuring a coefficient of determination $R^2 = 0.991$.

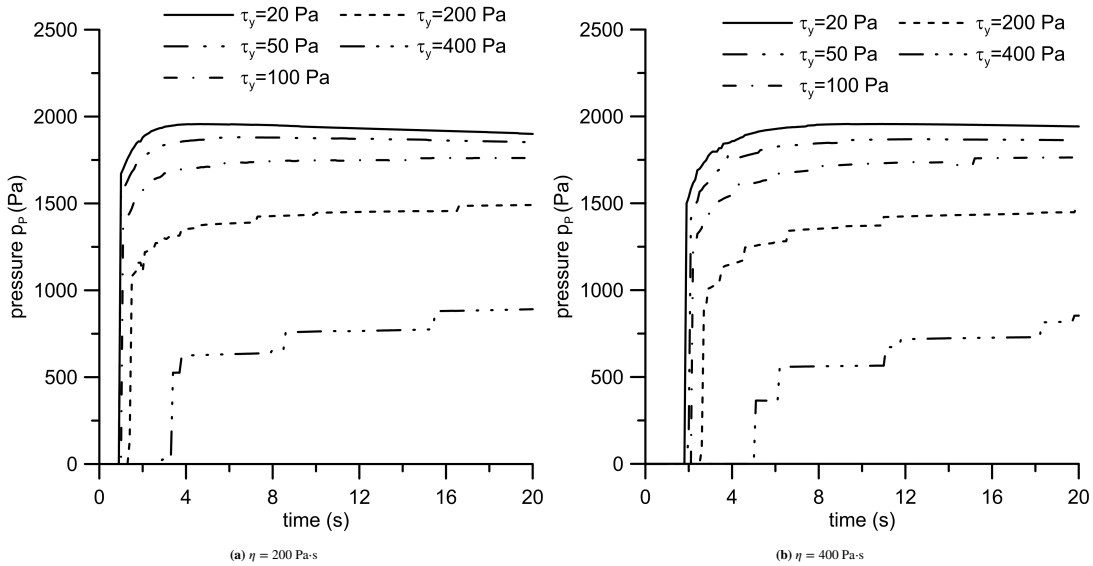

FIGURE 14 Time evolution of the pressure p_P at varying yield stress: (a) $\eta = 200$ Pa·s; (b) $\eta = 400$ Pa·s

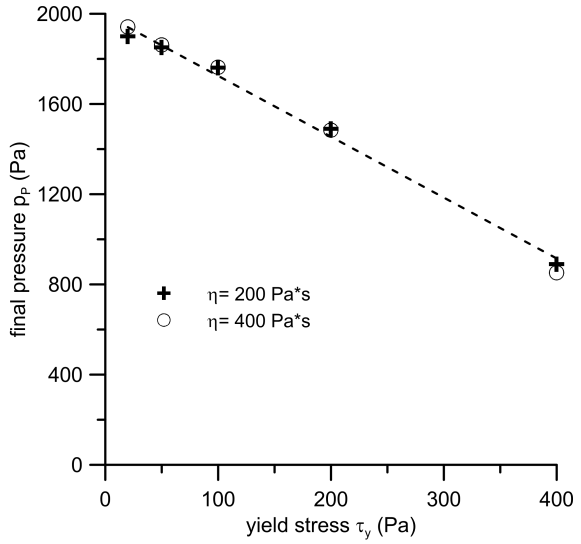

FIGURE 15 Dependence of the final p_P pressure on the yield stress

The above analysis of PFEM results suggests an alternative procedure to identify unambiguously both η and τ_y from measurements related to the dynamic impact of the liquefied soil mass on a rigid obstacle. Such a procedure requires the installation of a pressure transducer on the obstacle wall, and consists of two straightforward steps:

1. first, infer the yield stress τ_y from the final value of the pressure p_P at a given elevation h_P along the obstacle wall – where the mentioned pressure transducer shall have been installed. Owing to the linearity of dimensionless trend in Figure 16, two numerical simulations suffice to obtain the relevant calibration relationship. In particular, τ_y can be extracted from the dimensionless variable B, based on known values of ρ, H_0 and L_0;

2. the viscosity η is then derived as linked to the impact time Δt_P. Again, the linearity of the $\eta - \Delta t_P$ relationship (see Figure 13) makes two simulations with different viscosities sufficient to draw the linear trend relevant to calibration, based on the τ_y value identified in the previous step.

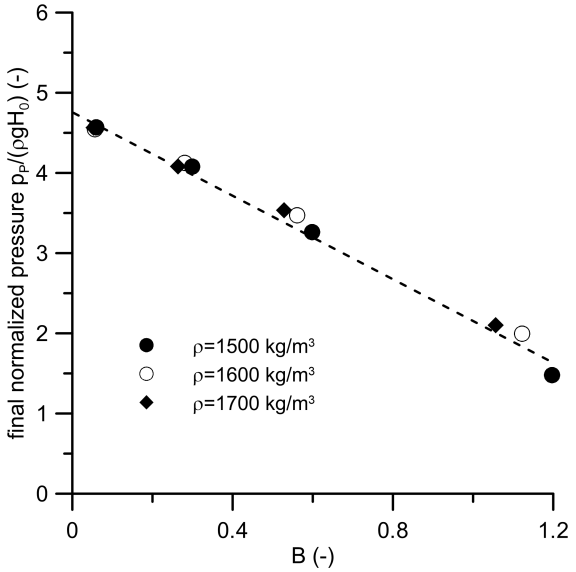

FIGURE 16 Dependence of the final normalised p_P pressure on B

The positioning of the obstacle (d_p) certainly affects the results of experiments/simulations, and deserves one last remark. Two extreme cases may be easily envisaged: (i) very large d_P, with the flowing mass attaining a stationary state before reaching the obstacle; (ii) very small d_P, with the flowing mass over-topping the obstacle during the *free fall* following the dam-breaking. In the intermediate settings considered in this study, the fluid mass first undergoes *free falling* right after dam breaking, then flows along the floor of the container up to hitting the obstacle: after the impact the liquefied sand bounces back and finds a final equilibrium through free oscillations damped out by its viscosity. In the simulations presented in the paper, the dynamics of the flowing mass is always of the latter type. Accordingly, for the range of viscosity, yield stress and density typical for fluidised geomaterials, over-topping will very hardly happen for d_P/L_0 values larger than 0.5. From a practical standpoint, it is thus recommended to design dam breaking experiments via preliminary CFD, so that the test can be made occur in conditions that will enable unambiguous interpretation (and identification of material parameters).

6 | CONCLUDING REMARKS

The interpretation of dam breaking tests on liquefied sands was reconsidered based on extensive CFD-PFEM parametric studies, in order to make the rheological characterisation of such water-soil mixtures more accurate and reliable. Along with model validation against literature data, it was first noted that, under the assumption of non-Newtonian Bingham behaviour, it would not be possible to unambiguously identify two material parameters (viscosity and yield stress) only based on the measurement of a single variable – usually, the evolving position of the tip of the liquefied mass.

PFEM simulations enabled to show that unambiguous parameter identification can be achieved by also monitoring the evolving aspect ratio (height over length) of the flowing mass or, even better, the fluid pressure on a rigid obstacle hit in the early stage of gravity-driven flow. Both recommendations can be very inexpensively implemented into current testing/interpretation procedures, with significant gain in terms of rheological characterisation. After verifying the suitability of the whole testing/-monitoring set-up, the proposed identification procedures imply themselves a very low number of experimental tests, as long as an appropriate CFD simulator is available for parallel back-analysis. The PFEM results presented in this work unveiled the simplicity (linearity) of certain relationships between relevant dimensionless groups, which fosters robust calibration of both rheological parameters: best case scenario is one dam breaking test and three CFD simulations to derive a unambiguous $\eta - \tau_y$ pair.

Future extensions of the proposed interpretation framework may include additional rheological factors, such as the pressure-dependence of the yield stress (frictional Bingham mixtures) and transient re-consolidation effects. The latter, in particular,

seems to be a topic for future fundamental research, regarding the large deformation simulation of two-phase porous media in the low-confinement regime.

ACKNOWLEDGEMENTS

The contribution of Alice Viti to numerical simulation activities in the preliminary stage of this research is warmly acknowledged.

References

1. De Groot MB, Bolton MD, Foray P, et al. Physics of liquefaction phenomena around marine structures. *Journal of Waterway, Port, Coastal, and Ocean Engineering.* 2006;132(4):227–243.

2. Hamada M. Case studies of liquefaction and lifeline performance during past earthquakes, vol. 1; Japanese case studies. *National Center for Earthquake Engineering Research, Technical Report.* 1992;92:341.

3. Bartlett SF, Youd TL. Empirical prediction of liquefaction-induced lateral spread. *Journal of Geotechnical Engineering.* 1995;121(4):316–329.

4. Cubrinovski M, Bray JD, Taylor M, et al. Soil liquefaction effects in the central business district during the February 2011 Christchurch earthquake. *Seismological Research Letters.* 2011;82(6):893–904.

5. Koppejan AW, Van Wamelen BM, Weinberg LJH. *Coastal flow slides in the Dutch province of Zeeland.* 1948.

6. Jeyapalan Jey K, Duncan J Michael, Seed H Bolton. Investigation of flow failures of tailings dams. *Journal of geotechnical engineering.* 1983;109(2):172–189.

7. Damgaard JS. Soil liquefaction around and its implications for pipelines. In: :5–6; 2004.

8. Finn WDL. Analysis of liquefaction induced displacements. In: :913–921; 1991.

9. Aydan O. Mechanical and numerical modeling of lateral spreading of liquefied soil. In: :881–6; 1995.

10. Towhata I, Sasaki Y, Tokida K, Matsumoto H, Tamari Y, Yamada K. Prediction of permanent displacement of liquefied ground by means of minimum energy principle. *Soils and Foundations.* 1992;32(3):97–116.

11. Boukpeti N, White DJ, Randolph MF. Analytical modelling of the steady flow of a submarine slide and consequent loading on a pipeline. *Géotechnique.* 2012;62(2):137.

12. Uzuoka R, Yashima A, Kawakami T, Konrad J-M. Fluid dynamics based prediction of liquefaction induced lateral spreading. *Computers and Geotechnics.* 1998;22(3-4):243–282.

13. Hwang JI, Kim CY, Chung CK, Kim MM. Viscous fluid characteristics of liquefied soils and behavior of piles subjected to flow of liquefied soils. *Soil Dynamics and Earthquake Engineering.* 2006;26(2-4):313–323.

14. Pastor M, Blanc Thomas, Haddad B, et al. Application of a SPH depth-integrated model to landslide run-out analysis. *Landslides.* 2014;11(5):793–812.

15. Hadush S, Yashima A, Uzuoka R, Moriguchi S, Sawada K. Liquefaction induced lateral spread analysis using the CIP method. *Computers and Geotechnics.* 2001;28(8):549–574.

16. Pastor M, Haddad B, Sorbino G, Cuomo S, Drempetic V. A depth-integrated, coupled SPH model for flow-like landslides and related phenomena. *International Journal for numerical and analytical methods in geomechanics.* 2009;33(2):143–172.

17. Huang Y, Zhang W, Mao W, Jin C. Flow analysis of liquefied soils based on smoothed particle hydrodynamics. *Natural hazards.* 2011;59(3):1547–1560.

18. Huang Y, Dai Z. Large deformation and failure simulations for geo-disasters using smoothed particle hydrodynamics method. *Engineering Geology.* 2014;168:86–97.

19. Schenkengel KU, Vrettos C. Simulation of liquefied sand by the Lattice Boltzmann method. *geotechnik*. 2014;37(2):96–104.

20. Idelsohn S.R., Oñate E., Pin F. Del. The particle finite element method: a powerful tool to solve incompressible flows with free-surfaces and breaking waves. *International Journal for Numerical Methods in Engineering*. 2004;61:964-989.

21. Oñate E., Franci A., Carbonell J.M.. Lagrangian formulation for finite element analysis of quasi-incompressible fluids with reduced mass losses. *International Journal for Numerical Methods in Fluids.* 2014;74 (10):699-731.

22. O'Brien J S, Julien PY. Laboratory analysis of mudflow properties. *Journal of hydraulic engineering.* 1988;114(8):877–887.

23. Stark Timothy D, Mesri Gholamreza. Undrained shear strength of liquefied sands for stability analysis. *Journal of Geotechnical Engineering.* 1992;118(11):1727–1747.

24. Olson Scott M, Stark Timothy D. Liquefied strength ratio from liquefaction flow failure case histories. *Canadian Geotechnical Journal.* 2002;39(3):629–647.

25. Scotto di Santolo A, Pellegrino AM, Evangelista A. Experimental study on the rheological behaviour of debris flow. *Natural Hazards and Earth System Sciences.* 2010;10(12):2507–2514.

26. Koos Erin, Linares-Guerrero Esperanza, Hunt Melany L, Brennen Christopher E. Rheological measurements of large particles in high shear rate flows. *Physics of Fluids.* 2012;24(1):013302.

27. Brezzi L, Cola S, Gabrieli F, Gidoni G. Spreading of kaolin and sand mixtures on a horizontal plane: physical experiments and SPH numerical modelling. *Procedia Engineering.* 2017;175:197–203.

28. Muller M, Tyrach J, Brunn PO. Rheological characterization of machine-applied plasters. *ZKG international.* 1999;52(5):252–258.

29. de Alba P, Ballestero TP. Residual strength after liquefaction: A rheological approach. *Soil Dynamics and Earthquake Engineering*. 2006;26(2-4):143–151.

30. Davidson MR, Khan NH, Yeow YL. Collapse of a cylinder of Bingham fluid. *ANZIAM Journal.* 2000;42:499–517.

31. Staron L, Lagrée PY, Ray P, Popinet S. Scaling laws for the slumping of a Bingham plastic fluid. *Journal of rheology.* 2013;57(4):1265–1280.

32. Kaitna R, Rickenmann D, Schatzmann M. Experimental study on rheologic behaviour of debris flow material. *Acta Geotechnica.* 2007;2(2):71–85.

33. Prime N, Dufour F, Darve F. Solid–fluid transition modelling in geomaterials and application to a mudflow interacting with an obstacle. *International Journal for Numerical and Analytical Methods in Geomechanics.* 2014;38(13):1341–1361.

34. Redaelli I, di Prisco C, Vescovi Dalila. A visco-elasto-plastic model for granular materials under simple shear conditions. *International journal for numerical and analytical methods in geomechanics.* 2016;40(1):80–104.

35. Moriguchi S, Borja RI, Yashima A, Sawada K. Estimating the impact force generated by granular flow on a rigid obstruction. *Acta Geotechnica.* 2009;4(1):57–71.

36. Nishimura S, Towhata I, Honda T. Laboratory shear tests on viscous nature of liquefied sand. *Soils and Foundations.* 2002;42(4):89–98.

37. Gallage CPK, Towhata I, Nishimura S. Laboratory investigation on rate-dependent properties of sand undergoing low confining effective stress. *Soils and foundations.* 2005;45(4):43–60.

38. Hadush S, Yashima A, Uzuoka R. Importance of viscous fluid characteristics in liquefaction induced lateral spreading analysis. *Computers and Geotechnics.* 2000;27(3):199–224.

39. Moriguchi S, Yashima A, Sawada K, Uzuoka R, Ito M. Numerical simulation of flow failure of geomaterials based on fluid dynamics. *Soils and Foundations.* 2005;45(2):155–165.

40. Pastor M, Blanc T, Pastor MJ. A depth-integrated viscoplastic model for dilatant saturated cohesive-frictional fluidized mixtures: application to fast catastrophic landslides. *Journal of Non-Newtonian Fluid Mechanics.* 2009;158(1-3):142–153.

41. Cremonesi M, Frangi A, Perego U. A Lagrangian finite element approach for the simulation of water-waves induced by landslides. *Computers & Structures.* 2011;89(11-12):1086–1093.

42. Cremonesi M, Frangi A, Perego U. A Lagrangian finite element approach for the analysis of fluid–structure interaction problems. *International Journal for Numerical Methods in Engineering.* 2010;84(5):610–630.

43. Idelsohn S.R., Oñate E., Pin F. Del, Calvo N.. Fluid-structure interaction using the particle finite element method. *Computer methods in applied mechanics and engineering.* 2006;195:2100-2113.

44. Franci A., Oñate E., Carbonell J.M.. Unified Lagrangian formulation for solid and fluid mechanics and FSI problems. *Computer Methods in Applied Mechanics and Engineering.* 2016;298:520-547.

45. Zhu M., Scott M. H.. Modeling fluid-structure interaction by the particle finite element method in OpenSees. *Computers and Structures.* 2014;132:12-21.

46. Oñate E., Idelsohn S.R., Celigueta M.A., Rossi R.. Advances in the particle finite element method for the analysis of fluidmultibody interaction and bed erosion in free surface flows. *Computer methods in applied mechanics and engineering.* 2008;197 (19-20):1777-1800.

47. Oñate E., Franci A., Carbonell J.M.. A particle finite element method for analysis of industrial forming processes. *Computational Mechanics.* 2014;54:85-107.

48. Cremonesi M., Ferri F., Perego U.. A basal slip model for Lagrangian finite element simulations of 3D landslides. *International Journal for Numerical and Analytical Methods in Geomechanics.* 2017;41:30-53.

49. Zhang X., Krabbenhoft K., Sheng D.. Particle Finite element analysis of the granular column collapse problem. *Granular Matter.* 2014;16:609-619.

50. Cremonesi M. A Lagrangian finite element method for the interaction between flexible structures and free surfaces fluid flows. PhD thesisPolitecnico di Milano2010.

51. Idelsohn Sergio R, Oñate Eugenio, Del Pin Facundo, Calvo Nestor. Fluid–structure interaction using the particle finite element method. *Computer Methods in Applied Mechanics and Engineering.* 2006;195(17-18):2100–2123.

52. Tezduyar T. E., Mittal S., Ray S. E., Shih R.. Incompressible flow computations with stabilized bilinear and linear equal-order-interpolation velocity-pressure elements. *Computer Methods in Applied Mechanics and Engineering.* 1992;95(2):221–242.

53. Ancey C. Plasticity and geophysical flows: a review. *Journal of Non-Newtonian Fluid Mechanics.* 2007;142(1-3):4–35.

54. Chen Y, Liu H, Wu H. Laboratory study on flow characteristics of liquefied and post-liquefied sand. *European Journal of Environmental and Civil Engineering.* 2013;17(sup1):s23–s32.

55. Horsten T. Pipe uplift in liquefied sands. Master's thesisDelft University of Technology2016.

56. Balmforth NJ, Craster RV, Perona P, Rust AC, Sassi R. Viscoplastic dam breaks and the Bostwick consistometer. *Journal of non-newtonian fluid mechanics.* 2007;142(1-3):63–78.

57. Hogg AJ, Matson GP. Slumps of viscoplastic fluids on slopes. *Journal of Non-Newtonian Fluid Mechanics.* 2009;158(1-3):101–112.

58. Matson GP, Hogg AJ. Two-dimensional dam break flows of Herschel–Bulkley fluids: the approach to the arrested state. *Journal of non-newtonian fluid mechanics.* 2007;142(1-3):79–94.

59. Hungr O. A model for the runout analysis of rapid flow slides, debris flows, and avalanches. *Canadian Geotechnical Journal.* 1995;32(4):610–623.